*Rev. Roum. Sci. Techn.– Électrotechn. et Énerg.*
Vol. **71**, *2*, pp. 217–222, Bucarest, 2026

# DSPACE REAL-TIME IMPLEMENTATION FOR CONTROL OF WIND-POWERED WATER PUMPING SYSTEM USING PERMANENT MAGNET SYNCHRONOUS GENERATOR

MEZIANE SALIMA[1], TOUFOUTI RIAD[1]

**Keywords: Wind energy; Induction motor; Permanent magnet synchronous generator; Centrifugal pump; Turbine; Wind pumping; Back-to-back converter; Indirect field-oriented control (FOC); dSpace1104.**

**This paper investigates the control of a wind-powered water-pumping system using a permanent-magnet synchronous generator (PMSG) driven by a wind-turbine emulator. The system consists of an induction motor powered by the PMSG through a back-to-back converter, with AC/DC and DC/AC conversion stages. The first section of this paper discusses the modeling and control of the wind-water pumping system, particularly in rural and remote regions. The performances of the turbine, the PMSG, and the IM Centrifugal pump are analyzed. Simulation results have demonstrated good performance and verified the validity of the proposed pumping system under different operating conditions, including wind speed, rotor reference speed, and torque pump variation. To validate the proposed control method, simulations were conducted in MATLAB/Simulink. In the second part, experimental validation was conducted using the dSPACE 1104 control board, enabling real-time data acquisition and control.**

## 1. INTRODUCTION

The generation of electric power from renewable energy sources, such as wind and solar, has attracted significant interest in recent years due to its potential in reducing environmental pollution and dependence on fossil fuels [1,4]. Among these sources, wind energy is considered one of the most promising alternatives for electricity generation, particularly in remote and rural areas, where it can be effectively employed for water pumping applications [1,4]. Water is crucial for human survival and rural development, and the increasing demand for irrigation and domestic water, coupled with declining rainfall and groundwater levels, has made mechanized water pumping indispensable [1,5]. Conventional water pumping systems, which rely on grid electricity or diesel engines, are progressively being replaced by photovoltaic (PV) and wind-powered systems, offering advantages such as lower operational costs, reduced noise, and decreased greenhouse gas emissions [6]. A typical wind-powered water pumping system consists of a wind turbine, an electric generator, power electronic converters, and an electric motor coupled with a centrifugal pump [4].

The use of the permanent magnet synchronous generator (PMSG) in these systems has gained attention due to its high efficiency, superior torque-to-inertia ratio, and the elimination of the gearbox [8,9]. Numerous studies have explored the performance of wind-powered pumping systems based on PMSGs, demonstrating favorable results under varying operating conditions. In [10], a control strategy was proposed for a system operating in southern Algeria, where a PMSG supplies power to a DC motor driving a centrifugal pump. In [11], a quasi-Z-source inverter was proposed for use with the PMSG, while [12] introduced an MPPT-based control approach for similar systems.

However, despite the effectiveness of DC motors, their higher maintenance requirements and operational costs have led to increased interest in induction motors (IMs), which are more reliable, robust, and cost-effective [13,15]. Although IMs are beneficial, they require advanced control techniques due to their nonlinear behavior [16,18]. Field-oriented control (FOC) and direct torque control (DTC) are two key techniques that enable decoupling of the rotor flux and electromagnetic torque, providing enhanced dynamic performance comparable to DC motors [19,20]. These techniques have been widely studied and applied to different types of induction motors for improving system performance.

In this study, the contribution is focused on the design and practical implementation of a wind-powered water pumping system using a PMSG and an induction motor controlled via FOC. The key innovation of this work is the experimental validation of the system, which has been implemented using the dSPACE 1104 platform for real-time control. This experimental approach demonstrates the system's performance in real conditions, addressing challenges in rural water pumping systems. By decoupling the flux and torque, the control strategy achieves efficient and reliable operation, with high dynamic performance similar to a DC motor drive. The results, both from simulation and experimental validation, highlight the effectiveness of the proposed system, offering a cost-effective and robust solution for rural water pumping applications.

## 2. DESCRIPTION OF WIND PUMPING SYSTEM

Figure 1 presents the structure of the wind water pumping system. It consists of a wind turbine, PMSG, a three-phase uncontrolled rectifier, a voltage source inverter, and an induction motor coupled to a centrifugal pump.

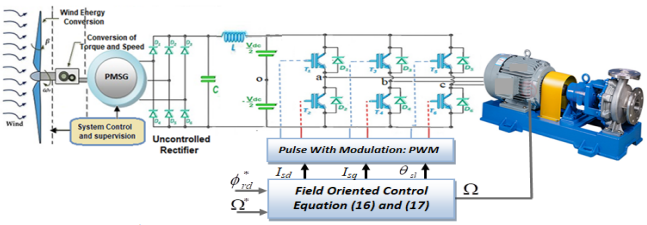


Fig.1 – Representation of the wind pumping system.

The wind turbine is directly and mechanically connected to the PMSG rotor shaft. The voltages obtained by PMSG are transmitted to the power electronic converter (uncontrolled rectifier to obtain an average DC-voltage, which is used to supply the inverter. The system IM centrifugal pump is controlled by field-oriented control.

### 2.1 WIND TURBINE

The wind power is converted into mechanical power. The mechanical power captured by the rotor blades, which subsequently drives the electrical generator, is expressed by (1) [1,13]:

[1]Department of Electrical Engineering, University of Souk Ahras, Laboratory of Electrical Engineering and Renewable Energies, Algeria.
E-mail: s.meziane@univ-soukahras.dz, riad.toufouti@univ-soukahras.dz

DOI: 10.59277/RRST-EE.2026.2.8

$$P_{tur} = \frac{1}{2}\rho S V^3 C_p(\lambda), \quad (1)$$

where $P_{tur}$: is the extracted power from the wind, ρ [kg/m$^3$] is the air density, $V$ [m/s] is the wind speed $S$ is the area swept by the rotor blades and $C_p$ is called the power coefficient, λ is a speed ratio,

$$\lambda = \frac{\Omega_t R}{V}, \quad (2)$$

$R$ is the radius, $\Omega_\tau$ is the mechanical angular velocity, respectively, of the wind turbine rotor. The power coefficient $C_p(\lambda,\beta)$, is [12]

$$,C_p(\lambda,\beta) = C_1\left(\frac{C_2}{\lambda_i} - C_3.\beta - C_4\right)e^{-\frac{C_5}{\lambda_i}} + C_6\lambda, \quad (3)$$

where β is the pitch angle, and $C_1$ to $C_6$, characteristic coefficients.

## 2.2 MODELING OF PMSG

The representation of the mathematical model of a three-phase PMSG in d-q reference frame can be given as shown in Fig. 2 [1,8,12]:

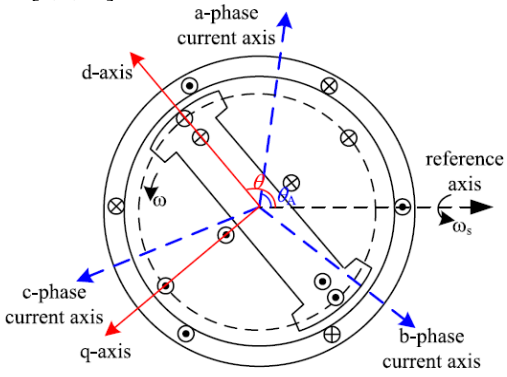


Fig. 2 –Representation of PMSG in dq and abc axis.

The stator flux and voltage of the PMSG are given by:

$$\begin{bmatrix}\psi_d\\ \psi_q\end{bmatrix} = \begin{bmatrix}L_d & 0\\ 0 & L_q\end{bmatrix}\begin{bmatrix}i_d\\ i_q\end{bmatrix} + \begin{bmatrix}\psi_v\\ 0\end{bmatrix}, \quad (4)$$

$$\begin{cases} V_d = R_s i_d + \frac{d\psi_d}{dt} - \omega_r \psi_q, \\ V_q = R_s i_q + \frac{d\psi_q}{dt} - \omega_r \psi_d, \end{cases} \quad (5)$$

where $i_d$, $i_q$, $V_d$, $V_q$, are the currents and voltages in the dq reference frame, $L_d$ and $L_q$ are the equivalent stator inductances in the dq synchronous reference frame, and $R_s$ stator resistance, the mechanical speed $\Omega = \omega_r/p$ .

$$T_{em} - T_r = J\frac{d\Omega}{dt} + f\Omega. \quad (6)$$

The electromagnetic torque is given by,

$$T_{em} = \frac{3p}{2}\left(\psi_f i_q + (L_d - L_q) i_d i_q\right), \quad (7)$$

where ψ is this $i$-th peak value of the flux created by the permanent magnet through the stator windings.

## 2.3 MODELING OF INDUCTION MOTOR

The complete model in stator fixed (α,β) reference frame can be written in the form for speed and flux control [15–22].

$$\begin{cases} \mathbf{x} = \mathbf{f}(\mathbf{x}) + \mathbf{g}(\mathbf{x})\mathbf{u}, \\ y_1 = h_1(x); y_2 = h_2(x), \end{cases} \quad (8)$$

where $\mathbf{x} = \begin{bmatrix} I_{s\alpha} & I_{s\beta} & \phi_{r\alpha} & \phi_{r\beta} & \Omega \end{bmatrix}^T$ is state vector has $n$ dimension, $\mathbf{u} = [u_{s\alpha} \quad u_{s\beta}]^T$, is a control signal has m dimension and $\mathbf{y} = [\Omega \quad (\phi_{r\alpha}{}^2 + \phi_{r\beta}{}^2)]^T$, is the measurement vector has $p$ dimension.

The state x belongs to the set $\{\mathbf{x} \in \Re^5 : \phi_{r\alpha}{}^2 + \phi_{r\beta}{}^2 \neq 0\}$ and the vector function $\mathbf{f}(\mathbf{x})$ is defined by:

$$\mathbf{f}(\boldsymbol{x}) = \begin{bmatrix} -\gamma I_{s\alpha} + \frac{K}{T_r}\phi_{r\alpha} - p\Omega k\phi_{r\beta} \\ -\gamma I_{s\beta} - p\Omega k\phi_{r\alpha} + \frac{K}{T_r}\phi_{r\beta} \\ \frac{M}{T_r} I_{s\alpha} - \frac{1}{T_r}\phi_{r\alpha} - p\Omega k\phi_{r\beta} \\ \frac{M}{T_r} I_{s\beta} + p\Omega k\phi_{r\alpha} - \frac{1}{T_r}\phi_{r\beta} \\ p\frac{M}{JL_r}\left(\phi_{r\alpha} I_{s\beta} - \phi_{r\beta} I_{s\alpha}\right) - \frac{1}{J}(T_L + f) \end{bmatrix}$$

$$[g] = \begin{bmatrix} g_1 \\ g_2 \end{bmatrix}^T = \begin{bmatrix} \frac{1}{\sigma L_s} & 0 & 0 & 0 & 0 \\ 0 & \frac{1}{\sigma L_s} & 0 & 0 & 0 \end{bmatrix}$$

$$T_r = \frac{L_r}{R_r}; \sigma = 1 - \frac{M^2}{L_s L_r}; K = \frac{M}{\sigma L_r L_s}; \gamma = \frac{R_s}{\sigma L_s} + \frac{R_r M^2}{\sigma L_r L_s}$$

where $I_{s\alpha}$, $I_{s\beta}$ denote the stator currents, $\phi_{r\alpha}$, $\phi_{r\beta}$ the rotor flux, $u_{s\alpha}$, $u_{s\beta}$ the stator voltages, $L_s$ , $L_r$ repectively the stator and rotor inductance, $R_s$ the stator resistance, $R_r$ the rotor resistance, Ω mechanical rotor speed, J as the motor inertia, $M$ for mutual inductance, f the friction coefficient, $p$ as the number of pole pairs, $T_L$ as the load torque, and $T_r$ for the rotor constant time.

The expressions for the electromagnetic torque and the dynamic speed are given by [28]:

$$T_{em} = \frac{pM}{L_r}\left(\phi_{rd} I_{sq} - \phi_{rq} I_{sd}\right), \quad (9)$$

$$J\frac{d\Omega}{dt} = T_{em} - T_r - f\Omega_r. \quad (10)$$

## 2.4 MODELING OF CENTRIFUGAL PUMP

The most widely used kind of pumping technology is the centrifugal pump, which can pump a large volume of water and has a relatively high efficiency due to its modular flexibility and ease of operation [2,3]. The pump represents the mechanical load of the induction motor. The mechanical equation of motor-pump system is given by,

$$K_m I_m - T_{pump} = J_m\frac{d\Omega}{dt} \quad (11)$$

with $J_m$ the moment of inertia of the group.

The relationships $H(Q)$ of total manometric head $H$ and the pump flow rate, and $T_r(Q)$ torque pump and manometric head H and the pump flow rate (Q) can be described by

$$H = a_0\omega^2 - a_1\omega Q - a_2 Q^2, \quad (12)$$

$$T_{pump} = b_0\omega^2 + b_1\omega Q - b_2 Q^2. \quad (13)$$

The power of the centrifugal pump can be given by (14):

$$P_{pump} = \rho g H, \quad (14)$$

where $a_0$, $a_1$, $a_2$, and $Q$ are manufacture pump coefficients. $b_0$, $b_1$, $b_2$ are constants depend on hydraulic par.

## 3. FIELD-ORIENTED CONTROL OF IM

FOC is a widely known vector control technique,

particularly suited for high-performance drive systems. The core principle of this method relies on the decoupling of flux and torque by controlling the stator current components, as depicted in Fig. 3. By aligning the d-axis of the Park coordinate system (d,q) with the rotor flux vector, the current along the d-axis controls the flux, while the current along the q-axis controls the torque [13–22].

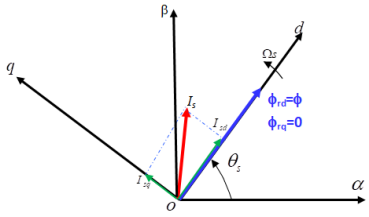


Fig.3 –Principal of field-oriented control.

The equations of the direct and quadrature are given by,

$$\begin{cases} \phi_{rd} = \phi_r, \\ \phi_{rq} = 0. \end{cases} \quad (15)$$

The equations of FOC are given by (16) and (17):

$$\omega_s = \omega + \frac{M_{sr} I_{sd}}{T_r \phi_r}, \quad (16)$$

$$T_{em} = \frac{3p}{2} \cdot \frac{M}{L_r} \phi_{rd} I_{sq}. \quad (17)$$

## 4. SIMULATION RESULTS

In this section, we present the simulation results in MATLAB/Simulink to verify and validate the good performance of the proposed pumping system, considering different operating conditions such as wind speed, rotor reference speed, and torque pump variation.

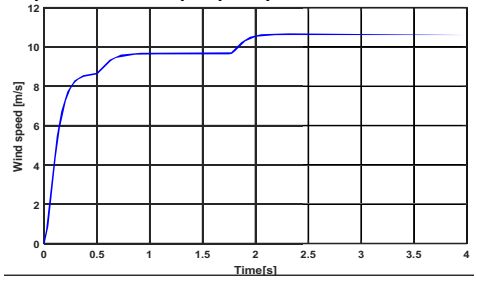


Fig. 4 – Wind speed variation.

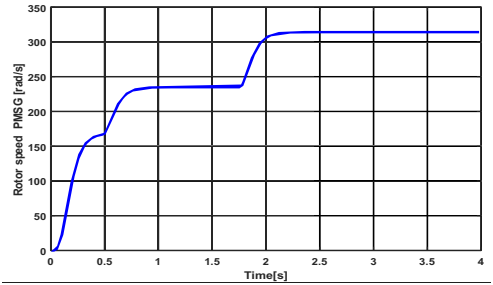


Fig. 5 – Speed of GSAP Variable .

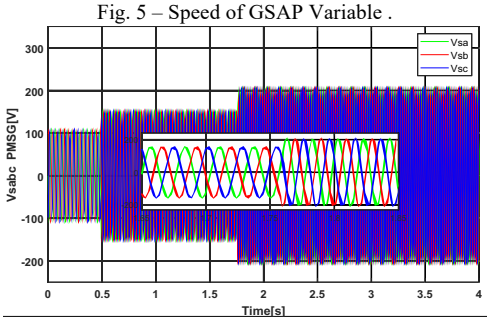


Fig. 6 – Stator voltage of GSAP.

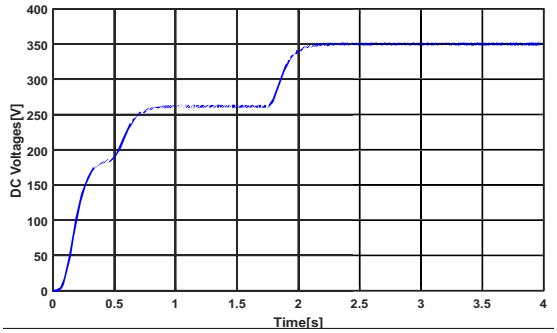


Fig. 7 – Output rectifier voltage.

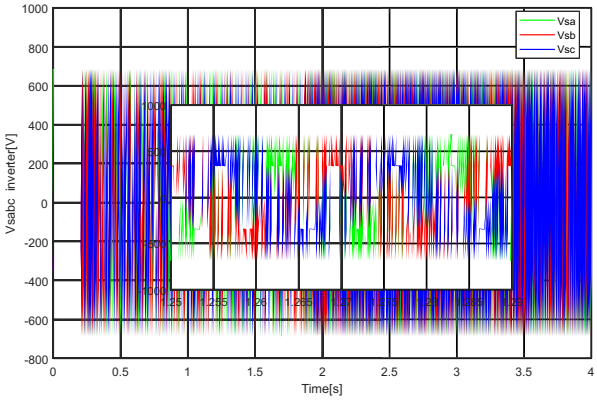


Fig.8 – Stator voltage of IM.

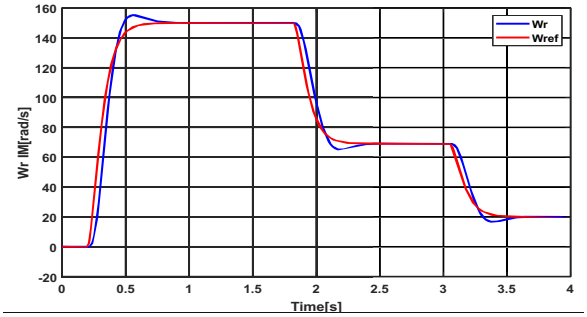


Fig. 9 – Rotor speed of IM.

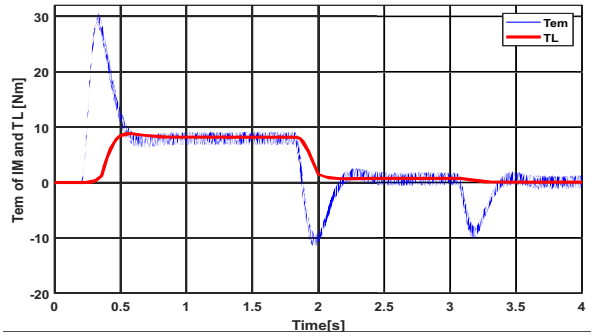


Fig. 10 –Torques of IM and pump.

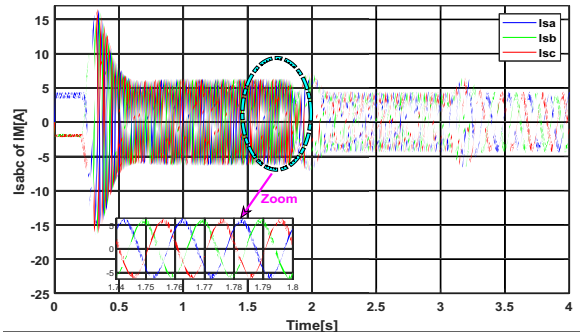


Fig. 11 – Stator current of IM.

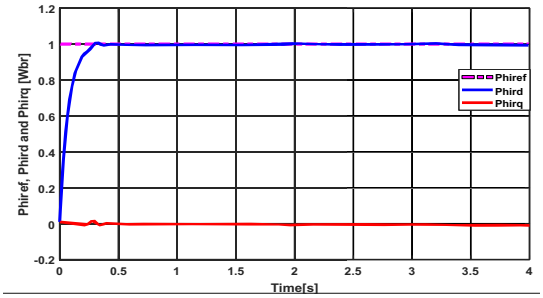


Fig. 12 – Direct and quadrature rotor flux.

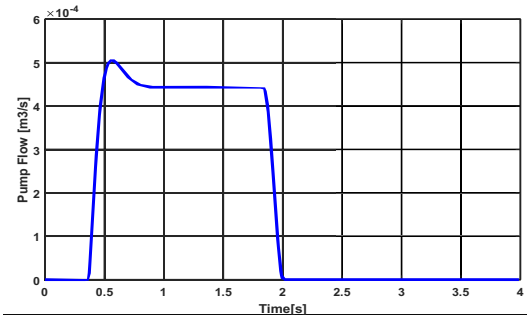


Fig. 13 – Pump Flow.

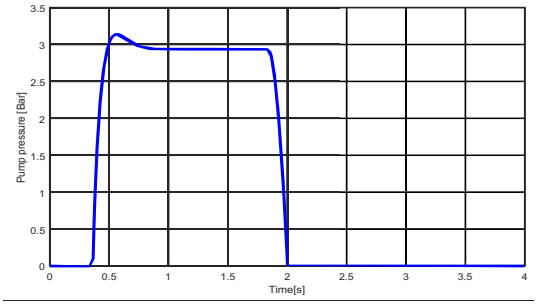


Fig. 14 – Pump pressure.

From the simulation results, we observe:

Figure 4: The wind speed follows an intermittent pattern, typical of wind energy, influencing the performance of the system. These fluctuations directly impact the speed of GSAP (wind turbine generator), as shown in the subsequent figures.

Figure 5: The rotor speed of the PMSG tracks the wind speed variations, demonstrating a direct relationship. The rotor speed exhibits a smooth increase with wind speed, showing minimal oscillations. The rotor speed of PMSG is synchronized with the wind speed.

Figure 6: The stator voltage of the GSAP is sinusoidal and balanced. The voltage response is proportional to the wind speed, confirming the robustness of the generator. The response time for voltage stabilization after a change in wind speed is less than 0.01 s, with ripples limited to less than 2% of the nominal voltage.

Figure 7: The DC output voltage of the rectifier reacts quickly to changes in rotor speed, stabilizing rapidly. Despite fluctuations in wind speed, the DC voltage stabilizes with minimal ripples. The response time for voltage regulation is less than 0.2 s, and the steady-state error is minimal, with voltage fluctuations within ±5%.

Figure 8: The stator voltage in the output inverter remains stable under varying conditions. The waveform is smooth with no visible ripples, indicating reliable power delivery to the motor. The response time for voltage stabilization is 0.2 s, confirming quick regulation. There are no sharp voltage deviations during load changes.

Figure 9: The rotor speed increases linearly with the reference speed, reaching a maximum value of 150 rad/s. The motor's speed tracks the reference speed with deviations less than 2% in the transient state and zero steady-state error from the desired value. The response time for speed adjustments is 0.2 s, ensuring smooth operation without significant ripples in speed.

Figure 10: The electromagnetic torque of the induction motor exhibits oscillations up to 30N.m during transient periods when the rotor speed changes. These ripples are expected during speed variations, with the transient period lasting for approximately 0.2 to 0.3 s. Once steady state is reached, the torque stabilizes at 8 Nm, tracking the pump's load torque, with minimal steady-state error (less than 0.5 Nm).

Figure 11: The stator current waveform of the induction motor is sinusoidal and stable, with no sharp peaks during load changes. The current peaks at 15 A during startup and settles to 5 A in steady state. The response time for current stabilization is 0.4 s, and the steady-state error is minimal, with a current ripple of less than ±1 A during operation.

Figure 12: The flux is well-controlled by the proposed control, with direct and quadrature flux components showing excellent decoupling. The flux error is minimal in the transient and study state, and the rotor flux tracks the reference flux exactly. The response time for flux stabilization is less than 0.1 seconds, and the steady-state error in flux is nearly negligible, that significant the quality of decoupling control ($\phi_r = \phi_{ref}$ and $\phi_{rq} = 0$).

Figure 13 illustrates the pump flow rate. The flow rate of the pump increases progressively, reaching approximately $4.5.10^{-4}$ m³/s when the rotor speed of IM reaches 150 rad/sec. When the rotor speed is below 150 rad/sec, the motor (MAS) rotates, but pumping stops at 2 s. To resume pumping, IFOC adjusts the reference speed.

Figure 14 represents the pump pressure for both cases. It is observed that the generated pressures are proportional to the flow rate, exhibiting similar trends with nearly identical scales.

## 5. HARDWARE IMPLEMENTATION

In our hardware implementation shown in Fig. 15, it mainly consists of a DC motor used to impose the driving torque on the PMSG orque of the wind turbine emulator. The PMSG is used to supply three phase squirrel cage induction via a voltage source inverter. One dSPACE DS1104 control board is used to control the inverter. This control board generates 6 PWM signals to control the voltage source inverter that imposes the needed stator current for the centrifugal pump.

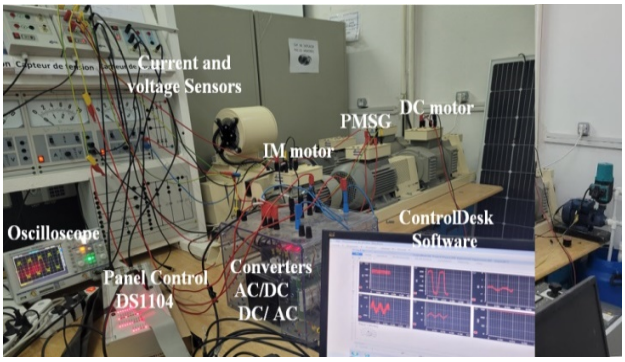


Fig. 15 – View of the experimental testing for IM drive system.

Figures 16 to 24 illustrate the results of the experimental validation, obtained using the DS1104 board, commonly used in research and development. These results are collected through control panel built into the dSPACE application software, ControlDesk assures real-time control of the experimental system [23].

The gate pulses generated for the IGBT of the DC/AC converter are shown in Fig. 16 and 17. In these figures, two pulses for PWM1: first in input gate driver generated microcontroller +5 V and +12 V in the output of the gate driver. Signals PWM1, PWM2, and PWM3, which has 20 kHZ, and the difference is only SPWM2 and SPWM3 signals leading respectively by 120° and 240°.

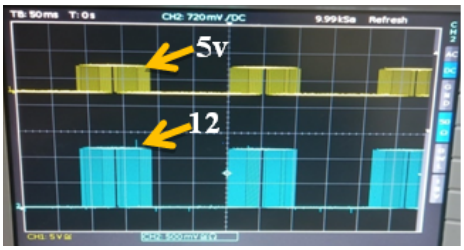


Fig. 16 – Input and output signals of gate drive.


Fig. 17 – Pulse of gate driver and drain source voltage.

The gate signal and drain-source voltage are shown in Fig. 17. Typically, the switching pattern of the gate signal: when the MOSFET is off (gate at 0 V), VDS is high, close to the supply voltage, and when the MOSFET is on. The voltage gate source (gate at $V_{GS}$ = 12 V).

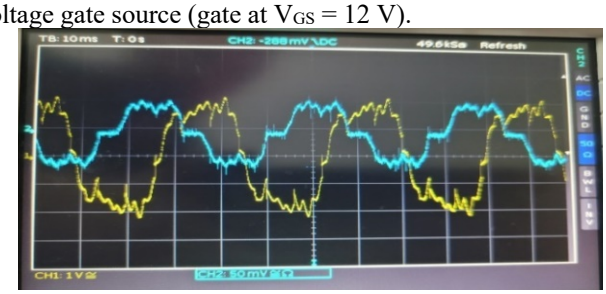

Fig. 18 – Stator current and voltage of PMSG.

Figure 18 illustrates a stator phase current of PMSG and show that the presence of the undulations is caused by the reluctance effect, the stator phase current of IM, and we also notice the effect of the PWM technique in this waveform. But the stator current is a sinusoidal fundamental wave.

Fig. 19 – Stator current and voltage of IM.

Figures 20 and 21 illustrate the voltage and current in the stator phase of PMSG. The stator voltage presents less undulation and is unaffected by these reluctance-induced current variations, and settles to 230 V.

The stator current exhibits undulations due to reluctance effects his value reaching 5 A. These variations occur because of changes in the magnetic reluctance, affecting the current.

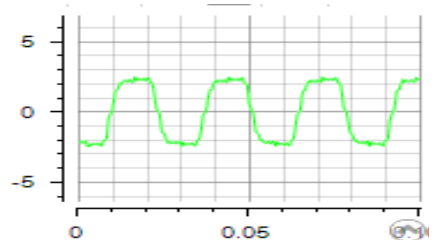


Fig. 20 – Stator voltage of PMSG.

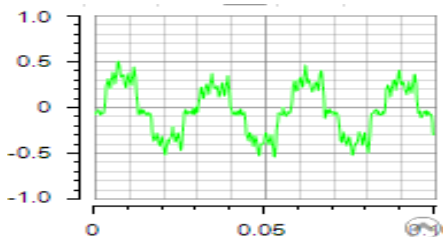


Fig. 21 – Stator current of PMSG.

Figures 22and 23 illustrate the voltage and current in the stator phase of induction motor.

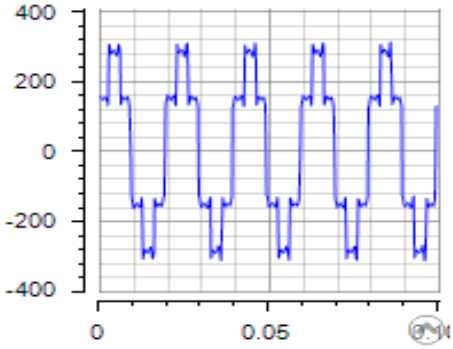


Fig. 22 – Stator voltage of IM

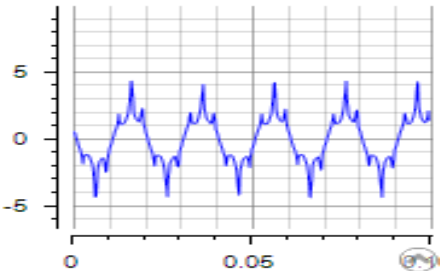


Fig. 23 – Stator current of IM

The stator voltage of the IM is shown as a square waveform due to the (PWM) technique, which is like the simulated voltage. The waveform has values: ($V_{dc}$/2, 2/3 $V_{dc}$, 0, -2/3 $V_{dc}$, -2/2 $V_{dc}$). However, the stator current exhibits harmonics caused by the influence of the current generated by the PMSG. These harmonics result in slight distortions in the current waveform, particularly under changing load conditions his value reaching 4 A.

## 5. COMPARISON STUDY

The quantitative comparison between simulation and experimental results, focusing on voltage and current, is presented in a table format. The small differences observed can be attributed to practical factors.

| Parameter | Simulation | Experimentation |
|---|---|---|
| Voltage of PMSG | Sinusoidal, ripple < 2%, stabilization time < 0.01 s | Smooth, stable at 230 V with minimal undulations |
| Current of PMSG | Sinusoidal, smooth behavior, maximum current ~5 A | Exhibits undulations due to reluctance effects, reaching 5 A |
| Voltage of (IM) | Smooth voltage, no visible ripples, stabilization time ~0.2 s | Square waveform due to PWM control, fluctuating between (Vdc/2, 2/3Vdc, 0, -2/3Vdc, -2/2Vdc) |
| Current of (IM) | Sinusoidal, peaks at 15 | Harmonics present, current up to 4 A, influenced by PMSG current |

## 6. CONCLUSIONS

This paper proposes an FOC strategy for a wind-powered water pumping system based on PMSG, driven by a wind turbine emulator. The IM is powered by the PMSG through a back-to-back converter. The simulation results confirm that the FOC enables effective decoupling of flux and torque, ensuring the stability of the motor-pump group speed and maintaining continuous pumping operation despite the variability of the wind resource. To further validate the wind energy conversion chain of the PMSG-based system, a hardware implementation is presented. The wind turbine emulator was developed using dSPACE. Future research will focus on experimental implementation of the proposed control system using predictive control.

## APPENDIX

PMSG parameters

$R_s$ = 1.4 Ω, $L_d$ = 6.6 mH, $L_q$ = 5.8 mH; $P$ = 1, $J$ = 0.00176.

IM parameters

$P_{IM}$ = 1.5 kW, $Rr$ = 3.81 Ω, $Rs$ = 4.85 Ω, $Ls$ = 0.274 H, $Lr$ = 0.274 H, $M$ = 0.258 H, $f$ = 0.00114, $J$ = 0.05 kg/m$^2$; $P$ = 2.

Pump parameters.

$P_{pump}$ = 1.1 kW, ω = 150 rad/s, $Q_{max} = 5.10^{-4}$ m$^3$/s, $H_{max}$ = 45 m, $a_0 = 3.6.10^{-3}$, $a_1 = 6.63.10^{-2}$, $a_2$ = 1.86, $b_0 = 1.73.10^{-4}$, $b_1$ = 0.0164, $b_2$ = 0.26.

## CREDIT AUTHORSHIP CONTRIBUTION STATEMENT

MEZIANE SALIMA: Theory, performed simulation, and results analysis.
TOUFOUTI RIAD: Presents the idea and Hardware Implementation.

*Received on 14 July 2025*

## REFERENCES


1. K. Rahrah, D. Rekioua, *Economic study of a solar/wind water pumping system with battery storage installed on the site of Bejaia*, pp. 1–10 (2015).
2. H. Bouzeriaa, C. Fethaa, T. Bahib, I. Abadliab, Z. Layateb, S. Lekhchinec, *Fuzzy logic space vector direct torque control of PMSM for photovoltaic water pumping system*, Energy Procedia, **74**, pp. 760–771 (2015).
3. S. Jaziri, K. Jemli, *Optimization of a photovoltaic powered water pumping system*, pp. 1–10 (2013).
4. S. Hammadi, N. Hidouri, L. Sbita, *A DTC-PMSG-PMSM drive scheme for an isolated wind turbine water pumping system*, International Journal of Research and Reviews in Electrical and Computer Engineering, **1**, *1*, pp. 1–6 (2011).
5. M. Girma, M. Molina, A. Assefa, *Feasibility study of a wind-powered water pumping system for rural Ethiopia*, AIMS Journal, pp. 1–10 (2015).
6. S.S. Chandela, M.N. Naik, R. Chandel, *Review of solar photovoltaic water pumping system technology for irrigation and community drinking water supplies*, Renewable and Sustainable Energy Reviews, pp. 1084–1099 (2015).
7. A. Lebsir, A. Bentounsi, M. Benbouzid, H. Mangel, *Electric generators fitted to wind turbine systems: An up-to-date comparative study*, Journal of Electrical Systems, **11**, *3*, pp. 281–295 (2015).
8. E. Mahersi, A. Kheder, *Adaptive backstepping control applied to wind PMSG system*, 2016 7th International Renewable Energy Congress (IREC), pp. 1–6 (2016).
9. C. Popa, N.S. Popa, F. Deliu, O. Cristea, I. Ciocioi, M.O. Popescu, *Analysis of wind turbine power output via modeling, simulation, and validation*, Rev. Roum. Sci. Techn. – Électrotechn. et Énerg., **70**, *2*, pp. 175–180 (2025).
10. J. Zhang, Z. Qi, J. Wen, *Control of water pumping driven by a wind turbine based on a quasi-Z source inverter*, pp. 1–10 (2020).
11. A. Dahbi, A. Harrouz, *MPPT control of wind turbine for water pumping system*, Applied Research Unit in Renewable Energies, Ghardaïa, Algeria, pp. 1–10 (2014).
12. Y. El Mourabit, A. Derouich, A. El Ghzizal, N. El Ouanjli, O. Zamzoum, *DTC-SVM control for permanent magnet synchronous generator-based variable speed wind turbine*, International Journal of Power Electronics and Drive Systems, **8**, *4*, pp. 1732–1740 (2017).
13. S. Meziane, R. Toufouti, L. Atarsia, *Non-linear adaptive control of induction motor drive for standalone photovoltaic water pumping system*, Handbook of Research on Modeling, Analysis, and Control of Complex Systems, IGI Global, pp. 450–476 (2021).
14. P. Vas, *Sensorless vector and direct torque control*, Oxford University Press, pp. 1–300 (1998).
15. K. Kendouci, B. Mazari, A. Akrad, R.M. Benhadri, *Integral backstepping approach and optimal two-stage Kalman filter for speed sensorless control of PMSM*, International Conference Tebessa, pp. 1–10 (2014).
16. M. Pietrzak-David, B. De Fornel, M.A. Purwoadi, *Nonlinear control for sensorless induction motor drives*, 9th International Conference on Power Electronics and Motion – EPE, pp. 1–10 (2000).
17. L. Atarsia, R. Toufouti, S. Meziane, *Control of wind water pumping using input-output feedback linearization technique*, International Conference on Digital Technologies and Applications, Springer, pp. 1–10 (2021).
18. S. Meziane, L. Atarsia, R. Toufouti, *A global stability of linearizing control of induction motor for PV water pumping application*, International Journal of System Dynamics Applications, pp. 1–10 (2018).
19. L. Khettache, M.R. Rezoug, A. Saadi, L. Sahraoui, *A novel design of a photovoltaic system based on a linear induction motor and reciprocating pump*, Rev. Roum. Sci. Techn. – Électrotechn. et Énerg., **70**, *1*, pp. 3–8 (2025).
20. R. Charles, V. Vinod, J. Anju, *Field-oriented control of doubly fed induction generator in wind power system*, Computational Intelligence and Computing Research (ICCIC), International Conference on IEEE, pp. 1–10 (2015).
21. A. Pantea, A. Sivert, A. Yazidi, F. Betin, S. Carriere, G.A. Capolino, *Efficient field-oriented control with power losses optimization of a six-phase induction generator for wind turbines*, Industrial Electronics Society, IECON 2016 – 42nd Annual Conference of the IEEE, pp. 1–10 (2016).
22. N. Rebei, B. Benghanem, A. Hmidet, O. Hasnaoui, *Study of photovoltaic water pumping system using scalar-DVC based control*, International Conference on Electrical Engineering and Software Applications, IEEE, pp. 1–8 (2013).
23. C.V. Suru, A. Bitoleanu, M. Popescu, M. Linca, F. Ravigan, *Particularities of rotor field orientation control implementation on industrial DSP systems*, Rev. Roum. Sci. Techn. – Électrotechn. et Énerg., **70**, *1*, pp. 15–20 (2025).